Optical frequency domain imaging with a rapidly swept laser in the 815-870 nm range

H. Lim, J. F. de Boer, B. H. Park, E. C. W. Lee, R. Yelin, and S. H. Yun

Harvard Medical School and Wellman Center for Photomedicine, Massachusetts General Hospital
50 Blossom Street, Boston, Massachusetts 02114
syun@hms.harvard.edu

Abstract: Optical frequency domain imaging (OFDI) in the 800-nm biological imaging window is demonstrated by using a novel wavelength-swept laser source. The laser output is tuned continuously from 815 to 870 nm at a 43.2-kHz repetition rate with 7-mW average power. Axial resolution of 10-μm in biological tissue and peak sensitivity of 96 dB are achieved. *In vivo* imaging of *Xenopus laevis* is demonstrated with an acquisition speed of 84 frames per second (512 axial lines per frame). This new imaging technique may prove useful in comprehensive retinal screening for medical diagnosis and contrast-agent-based imaging for biological investigations.

OCIS codes: (110.4500) Optical coherence tomography; (120.3180) Interferometry; (140.3600) Lasers, tunable; (170.3880) Medical and biological imaging; (170.4470) Ophthalmology; (330.4460) Ophthalmic optics

References and links

1. D. Huang, E. A. Swanson, C. P. Lin, J. S. Schuman, W. G. Stinson, W. Chang, M. R. Hee, T. Flotte, K. Gregory, C. A. Puliafito, and J. G. Fujimoto, "Optical coherence tomography," Science **254**, 1178-1181 (1991).
2. W. Sorin, *Optical reflectometry for component characterization*, in *Fiber Optic Test and Measurement* D. Derickson, ed., (Prentice Hall PTR, 1998).
3. A. F. Fercher, C. K. Hitzenberger, G. Kamp, and S. Y. Elzaiat, "Measurement of intraocular distances by backscattering spectral interferometry," Opt. Commun. **117**, 43-48 (1995).
4. S. R. Chinn, E. A. Swanson, and J. G. Fujimoto, "Optical coherence tomography using a frequency-tunable optical source," Opt. Lett. **22**, 340-342 (1997).
5. B. Golubovic, B. E. Bouma, G. J. Tearney, and J. G. Fujimoto, "Optical frequency-domain reflectometry using rapid wavelength tuning of a Cr/sup 4+/:forsterite laser," Opt. Lett. **22**, 1704-1706 (1997).
6. S. H. Yun, G. J. Tearney, J. F. de Boer, N. Iftimia, and B. E. Bouma, "High-speed optical frequency-domain imaging," Opt. Express **11**, 2953-2963 (2003).
7. M. A. Choma, M. V. Sarunic, C. H. Yang, and J. A. Izatt, "Sensitivity advantage of swept source and Fourier domain optical coherence tomography," Opt. Express **11**, 2183-2189 (2003).
8. R. Huber, M. Wojtkowski, and J. G. Fujimoto, "Fourier Domain Mode Locking (FDML): A new laser operating regime and applications for optical coherence tomography," Opt. Express **14,** 3225-3237 (2006).
9. R. Huber, M. Wojtkowski, K. Taira, J. G. Fujimoto, and K. Hsu, "Amplified, frequency swept lasers for frequency domain reflectometry and OCT imaging: design and scaling principles," Opt. Express **13**, 3513-3528 (2005).
10. B. J. Vakoc, S. H. Yun, J. F. de Boer, G. J. Tearney, and B. E. Bouma, "Phase-resolved optical frequency domain imaging," Opt. Express **13,** 5483-5493 (2005).
11. Y. Yasuno, V. D. Madjarova, S. Makita, M. Akiba, A. Morosawa, C. Chong, T. Sakai, K. P. Chan, M. Itoh, and T. Yatagai, "Three-dimensional and high-speed swept-source optical coherence tomography for in vivo investigation of human anterior eye segments," Opt. Express **13**, 10652-10664 (2005).
12. J. Zhang, W. G. Jung, J. S. Nelson, and Z. P. Chen, "Full range polarization-sensitive Fourier domain optical coherence tomography," Opt. Express **12**, 6033-6039 (2004).

#70059 - $15.00 USD Received 18 April 2006; revised 9 June 2006; accepted 14 June 2006

13. M. V. Sarunic, S. Weinberg, and J. A. Izatt, "Full-field swept-source phase microscopy," Opt. Lett. **31**, 1462-1646 (2006).
14. W. Y. Oh, S. H. Yun, B. J. Vakoc, G. J. Tearney, and B. E. Bouma, "Ultrahigh-speed optical frequency domain imaging and application to ablation monitoring," Appl. Phys. Lett. 103902 (2006).
15. E. C. W. Lee, J. F. de Boer, M. Mujat, H. Lim, and S. H. Yun, "In vivo optical frequency domain imaging of human retina and choroid," Opt. Express **14**, 4403-4411 (2006),
16. M. R. Hee, J. A. Izatt, E. A. Swanson, D. Huang, J. S. Schuman, C. P. Lin, C. A. Puliafito, and J. G. Fujimoto, "Optical coherence tomography of the human retina," Arch. Ophthalmol. **113**, 325-32 (1995).
17. W. Drexler, "Ultrahigh-resolution optical coherence tomography," J. Biomed. Opt. **9**, 47-74 (2004).
18. M. Wojtkowski, R. Leitgeb, A. Kowalczyk, T. Bajraszewski, A. F. Fercher, "In vivo human retinal imaging by fourier domain optical coherence tomography," J. Biomed. Opt. **7**, 457-463 (2002).
19. N. Nassif, B. Cense, B. Park, M. Pierce, S. Yun, B. Bouma, G. Tearney, T. Chen, and J. de Boer, "In vivo high-resolution video-rate spectral-domain optical coherence tomography of the human retina and optic nerve," Opt. Express **12**, 367-376 (2004).
20. S. A. Boppart, A. L. Oldenburg, C. Xu, and D. L. Mark, "Optical probes and techniques for molecular contrast enhancement in coherence imaging," J. Biomed. Opt. **10**, 041208 (2005).
21. S. H. Yun, G. J. Tearney, J. F. de Boer, and B. E. Bouma, "Removing the depth-degeneracy in optical frequency domain imaging with frequency shifting," Opt. Express **12**, 4822-4828 (2004),
22. S. H. Yun, G. J. Tearney, J. F. de Boer, and B. E. Bouma, "Motion artifacts in optical coherence tomography with frequency-domain ranging," Opt. Express **12,** 2977-2998 (2004).
23. S. H. Yun, C. Boudoux, G. J. Tearney, and B. E. Bouma, "High-speed wavelength-swept semiconductor laser with a polygon-scanner-based wavelength filter," Opt. Lett. **28**, 1981-1983 (2003).
24. M. Fukuda, *Reliability and Degradation of Semiconductor Lasers and LEDs*, (Artech House Publishers, 1991).
25. B. M. Green, K. K. Chu, E. M. Chumbes, J. A. Smart, J. R. Shealy, and L. F. Eastman, "The effect of surface passivation on the microwave characteristicsof undoped AlGaN/GaN HEMTs," IEEE Electron. Dev. Lett. **21**, 268-270 (2000).
26. B. H. Park, M. C. Pierce, B. Cense, S. H. Yun, M. Mujat, G. J. Tearney, B. E. Bouma, and J. F. de Boer, "Real-time fiber-based multi-functional spectral-domain optical coherence tomography at 1.3 μm," Opt. Express **13**, 3931-3944 (2005).
27. S. A. Boppart, G. J. Tearney, B. E. Bouma, J. F. Southern, M. E. Brezinski, and J. G. Fujimoto, "Noninvasive assessment of the developing Xenopus cardiovascular system using optical coherence tomography," Proc. Natl. Acad. Sci. U.S.A. **94**, 4256-4261 (1997).
28. K. D. Rao, M. A. Choma, S. Yazdanfar, A. M. Rollins, and J. A. Izatt, "Molecular contrast in optical coherence tomography by use of a pump-probe technique," Opt. Lett. **28**, 340-342 (2003).
29. C. H. Yang, L. E. L. McGuckin, J. D. Simon, M. A. Choma, B. E. Applegate, and J. A. Izatt, "Spectral triangulation molecular contrast optical coherence tomography with indocyanine green as the contrast agent," Opt. Lett. **29**, 2016-2018 (2004).
30. H. Cang, T. Sun, Z. Y. Li, J. Y. Chen, B. J. Wiley, Y. N. Xia, and X. D. Li, "Gold nanocages as contrast agents for spectroscopic optical coherence tomography," Opt. Lett. **30**, 3048-3050 (2005).

1. Introduction

Optical coherence tomography (OCT) is an optical imaging modality that provides depth-resolved morphological information [1]. Optical frequency domain imaging (OFDI), also known as swept-source OCT, is an emerging new technique for OCT based on swept wavelength interferometry. OFDI offers several advantages, such as higher sensitivity and imaging speed, over conventional time-domain technique. In OFDI, the sample's axial scattering profile is obtained by detecting spectrally resolved interference as the source wavelength is swept rapidly. Since the detector signal at each wavelength (λ) is directly related, in amplitude and phase, to a corresponding spatial modulation of the refractive index distribution, with a spatial frequency of $2/\lambda$, Fourier transformation of the interference signal produces a depth profile (A-line). This frequency-domain method has been well-known in metrology [2, 3] and its feasibility for imaging has been demonstrated [4, 5]. However, only recently has the significance in high-speed biomedical imaging become evident [6, 7]. To date, developments in OFDI have been focused in a 1300-nm biological window for deep tissue imaging [6-14], and more recently in a 1060-nm range [15]. OFDI at shorter wavelengths,

#70059 - $15.00 USD Received 18 April 2006; revised 9 June 2006; accepted 14 June 2006

particularly 700-900 nm, would be of considerable interest for retinal [16-19] and molecular-contrast imaging [20]; however, the unavailability of appropriate light sources with broad tuning range, high sweep speed, and high output power has hampered the development of OFDI in the application-rich imaging window. Compared to spectral-domain OCT in the 800-nm range [8, 9], OFDI promises to offer a number of distinct advantages, such as longer depth ranges [21], simpler polarization-sensitive implementation [12], higher imaging speed [8, 14], and lower sensitivity to motion [22].

In this paper, we present the first demonstration of a biomedical OFDI system operating in the 800-nm imaging window. The system offers a high resolution (10 μm in tissue), high imaging speed (43,200 axial scans per second), and high sensitivity (96 dB maximum). The key-enabling element of the system is a wavelength swept laser developed with a state-of-the-art, commercially-available semiconductor optical amplifier. To demonstrate the system's capability for biomedical imaging, we present an OFDI movie of *Xenopus laevis* tadpole *in vivo*.

2. Wavelength-swept laser

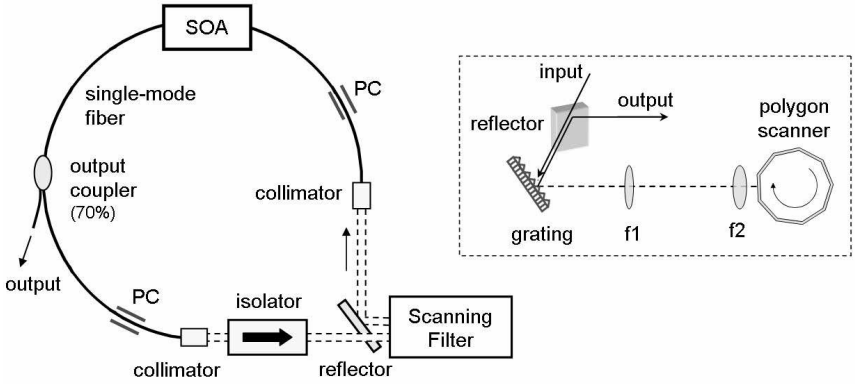

Fig. 1. Schematic of the wavelength-swept laser source. SOA; semiconductor optical amplifier. (Inset) the intracavity wavelength scanning filter.

Figure 1 depicts the experimental setup. The swept laser has a unidirectional ring cavity with a free-space isolator (IO-5-NIR, OFR Inc.). The gain medium is a fiber-coupled state-of-the-art semiconductor optical amplifier (SOA-372-850-SM, Superlum Diodes Ltd.) with high gain and broad bandwidth that recently has become available commercially. The intracavity spectral filter [23] comprises a diffractive grating (830 grooves/mm), two achromatic lenses in the 4*f* configuration, and a 72-facet gold-coated polygon mirror (Lincoln Lasers, Inc.). The facet size is 2.77 mm. We rotated the polygonal mirror at 600 revolutions per second to produce unidirectional sweeps from short to long wavelengths at a 43.2-kHz repetition rate. To facilitate unidirectional oscillation, we displaced the beams entering and exiting the filter vertically from each other by adjusting the alignment in the filter. The beams were separated by a metal mirror placed in front of the grating. The focal length of the fiber collimators (PAF-X-5, OFR, Inc.) is 4.6 mm, yielding a beam size of ~0.6 mm FWHM (full width at half maxima) at the grating. The beam incident angle to the grating is 67 +/- 5 deg. The focal lengths of the two lenses in the telescope are 75 (f_1) and 40 (f_2) mm, respectively. A simple calculation [23] yields a free-spectral range of 55 nm and FWHM bandwidth of 0.21 nm. The laser output is obtained via a 70% port of a fiber-optic coupler. Two polarization controllers (PC's) were used to maximize the output power and tuning range.

We measured the spectral and temporal characteristics of the laser output at a 43.2-kHz sweep rate. The SOA was driven with an injection current of 110 mA. Figure 2(a) shows the

#70059 - $15.00 USD Received 18 April 2006; revised 9 June 2006; accepted 14 June 2006

output spectrum measured with an optical spectrum analyzer in the peak-hold mode at a resolution bandwidth of 0.1 nm. The total tuning range is 55 nm from 815 to 870 nm with a FWHM bandwidth of 38 nm. No significant spectral ripple was observed in the peak-hold output spectrum. The stability of the output power is apparent in the single-shot oscilloscope trace (detection bandwidth: 20 MHz) shown in Fig. 2(b). The power variation between tuning cycles is less than 1%. The instantaneous laser emission contains multiple longitudinal modes; the measured coherence length [Fig. 4(b)] indicates that the FWHM linewidth is 0.085 nm, considerably smaller than the theoretical filter bandwidth of 0.21 nm. We measured the intensity noise of the laser output using an electrical spectrum analyzer (Model E4411B, Agilent) and a low-gain silicon detector, which was less than −130 dB/Hz in the frequency range from 2 to 90 MHz, whereas the noise level increases toward DC, primarily due to envelop modulation in the sweep operation. The fundamental longitudinal mode beat note appeared at 91 MHz. The average output power measured with a power meter was 7 mW. The output contains broadband amplified spontaneous emission (ASE) generated from the SOA. To determine the ASE level, we measured the backward-propagating ASE power by inserting a thin slide glass in the cavity between the filter and SOA. The measured ASE power was 0.56 mW, ~8% of the total laser output power.

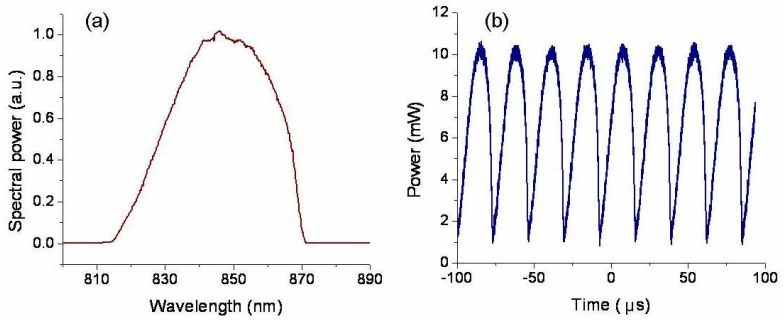

Fig. 2. Output characteristics of the wavelength-swept laser. (a) Peak-hold output spectrum on logarithmic (dashed) and linear (solid) scales. (b) Time-domain trace at a 43.2 kHz sweep rate and 7 mW average power.

The large output coupling ratio of our laser (70%) ensured that the peak power at the SOA does not exceed the specified optical damage threshold of 20 mW at the output fiber that corresponds to 50 mW at the gain chip. When this condition was not satisfied in another SOA devices tested, we observed sudden catastrophic optical damage (COD) of the SOA. The COD was localized at the output facet of the chip, as evident from >30-dB reduction in amplified spontaneous emission (ASE) in the forward direction but a minor change in the backward direction. In other devices, slowly progressing degradation (increasing loss) was also observed in the time scale of hours and days (depending on the driving condition,) decreasing the optical gain and eventually frustrating lasing. The COD in high-power 800-nm semiconductor devices has been extensively studied, and a primary mechanism is known to be a thermally-induced material meltdown due to high optical and current densities at the output facet [24]. Slow degradation may be attributed to the migration of dark line defect facilitated into the active region by an elevated temperature in the device [24]. The 800-nm devices based on AlGaAs multiple-quantum well are known to have lower COD threshold than aluminium-free 1060- or 1300-nm semiconductor devices. A number of potential solutions may improve the reliability of the gain chip, including surface passivation [25] and waveguide designs. This will allow higher gain and bandwidth to be achieved, leading to higher output power and tuning range in a swept laser. As another solution, a feedback control may be implemented to modulate the driving current or cavity loss in response to the monitored instantaneous output

#70059 - $15.00 USD Received 18 April 2006; revised 9 June 2006; accepted 14 June 2006

power. This active control would limit the injection current at the wavelengths with high gain, but permit more current at the wavelengths with low gain, which maximizes the tuning range. In our laser, high output coupling decreases the intracavity power to avoid the COD and slow degradation, leading to a stable operation observed over one month.

3. Optical frequency domain imaging

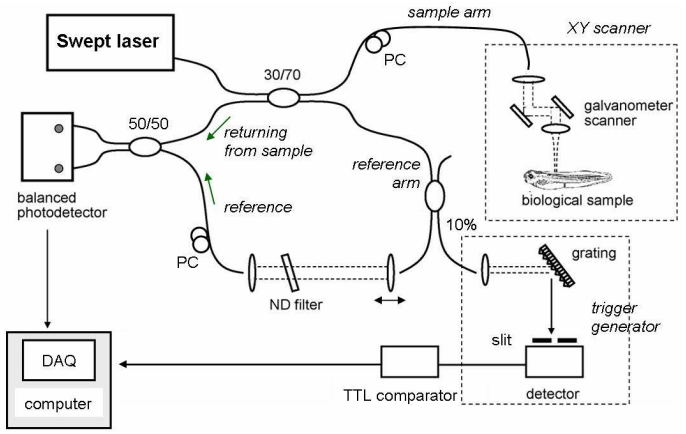

Fig. 3. Schematic of the optical frequency domain imaging system.

We constructed an OFDI system using the wavelength-swept laser. A schematic of the system is shown in Fig. 3. The laser output is split into two paths in an interferometer by a 30/70 coupler. One path (a 30% port, "sample arm") contains a two-axis galvanometer beam scanner and an achromatic imaging lens (f = 30 mm). The other path, "a reference arm," provides a reference beam. In contrast to conventional Michelson interferometer using a reflective reference arm [6-8], the transmissive reference arm design facilitates power-efficient dual balanced detection without Faraday circulators. The signal beam returning from the sample is combined with the reference beam at a 50/50 coupler to produce interference. The interference signal is detected with a dual-balanced silicon receiver (DC-80 MHz, 1807-FS, New Focus). The receiver output is low-pass filtered (35 MHz) and digitized at a sampling rate of 100 MS/s with a 14-bit data acquisition board (DAQ, NI-5122, National instruments). A small portion (10%) of the reference beam is tapped and detected through a grating filter to provide triggers to the DAQ board [6]. The short trigger rearm time of the board, 2 μs, provides a 100% sampling duty cycle. During each wavelength sweep or A-line scan, a total of 2048 samples are acquired. The sampled data are initially stored in an on-board memory. Upon collecting a desired number of A-line scans, the data set is transferred to a host personal computer, either to the computer memory for real-time processing and display or to the hard disk for post processing. When only a single frame (512 A-lines) is acquired at a time, the system is capable of processing and displaying the images in real time at a frame refresh rate of 5 Hz. The on-line data control and display software was written in Visual C++ [26]. Larger data sets are stored in the 256 MB on-board memory. This allowed us to acquire maximum 65,536 A-line scans consecutively for 1.3 sec, corresponding to 128 images. Post data processing involves reference subtraction, apodization, *k*-space interpolation, dispersion compensation, followed by Fourier transformation. The methods for each of this process have been described [6, 9, 15, 19]. For apodization, we used a custom window function with a square-top bell shape, but other standard functions such as Gaussian or Humming were found to work equally well**.**

#70059 - $15.00 USD Received 18 April 2006; revised 9 June 2006; accepted 14 June 2006

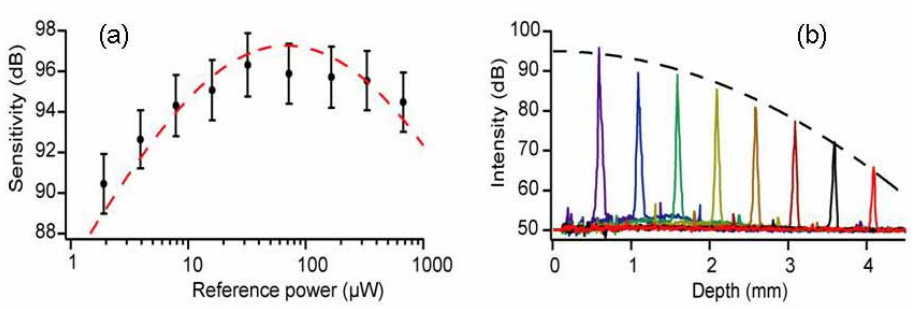

Fig. 4. Sensitivity of the OFDI system as a function of the reference power (a) and depth (b), measured with an attenuated mirror with a -50 dB reflectivity. The dashed lines are theoretical fits.

To characterize and optimize the system, we investigated the axial point spread function by measuring the A-line profile of a partially-reflecting mirror sample (-50 dB reflectivity). Figure 4(a) depicts the sensitivity of the system measured as a function of the reference optical power. The reference power was varied by using a neutral density (ND) filter in the reference arm. Throughout this measurement, the path length difference between the sample and reference arms was maintained at 0.6 mm. The maximum optical power available at the output of the XY scanner was 2.4 mW. With a ND filter (OD=2.5) and 3-dB single-pass loss in the scanner, the optical power returning from the attenuated sample mirror was 3.0 nW at each port of the 50/50 coupler. The sensitivity values were determined by adding the sample attenuation (50 dB) to the measured SNR. The reference power was measured at one of the ports of the 50/50 coupler, which is an average reference power arriving at each photodiode. The result indicates that the optimal range of the reference power is between 30 and 200 μW, and the best sensitivity is ~96 dB.

To understand this result, we used a theoretical model described in [6]. The sensitivity in the unit of decibel can be expressed as: $S_{dB} = S_0 - 10\log_{10}(1 + a/P_r + P_r/b) - \Delta$, where S_0 denotes the shot-noise limited sensitivity, P_r is the reference power level, a and b correspond to the reference power levels at which thermal and intensity noise, respectively, are equal in magnitude to shot noise, and Δ is a fitting parameter associated with other contributions to the loss of sensitivity. We took into account amplified spontaneous emission in the output of the laser to estimate S_0 to be 107 dB [6] and determined a = 17 μW from the detector noise level (3.3 pW/√Hz). From the best fit to the experimental data [dotted line in Fig. 4(a)], we obtained b = 280 μW and Δ = 8 dB. From the value of b and the measured relative intensity noise of the laser (-130 dB/Hz), the common-noise suppression efficiency of the balanced receiver is calculated to be 18 dB, 7 dB lower than the vendor's specification. We found that the discrepancy is mainly due to the unequal and wavelength-dependent splitting ratio of the nominally 50/50 fiber coupler. We attribute nonzero Δ to several factors, including the flat-spectrum assumption of our model, wavelength-dependent polarization mismatch between the sample and reference beams, and the apodization step in data processing [15].

Due to a finite coherence length of the laser output, the sensitivity decreases as the interferometric delay increases. We measured axial point spread functions at various depths of the sample mirror by changing the delay in the reference arm. The reference power was maintained at 100 μW per photodiode. Figure 4(b) illustrates the results. Each axial profile was corrected by measuring the background obtained while blocking the sample arm, and by subtracting this noise floor from each depth profile. This process flattens the noise level that otherwise varies with frequency, or depth, by ~2 dB. We converted the measured intensity into the sensitivity by adding the sample attenuation of 50 dB. The sensitivity drops by 6 dB at a depth of 1.9 mm. A Gaussian fit (dashed line) indicates the instantaneous laser linewidth to be 0.085 nm. The FWHM of the axial profile (linear amplitude) is approximately 14 μm in

#70059 - $15.00 USD Received 18 April 2006; revised 9 June 2006; accepted 14 June 2006

the depth from 0 to 3 mm, corresponding to a 10-μm axial resolution in biological tissue (refractive index, $n \approx 1.35$). From the source spectrum [Fig. 2(a)] and the window function we used, we obtain a theoretical axial resolution of 10.5 μm in air. The relatively large discrepancy is largely due to signal processing errors in *k*-space interpolation and dispersion compensation. These errors also resulted in considerable sidelobes in the axial profile, that are 10 dB below the peak. We expect the resolution to be enhanced by improving calibration of the source tuning curve and interferometer dispersion. Transform-limited axial resolutions have been achieved in previous OFDI systems [9,10]. Small echoes seen near the noise floor are due to double-pass reflection at the ND filter in the reference arm.

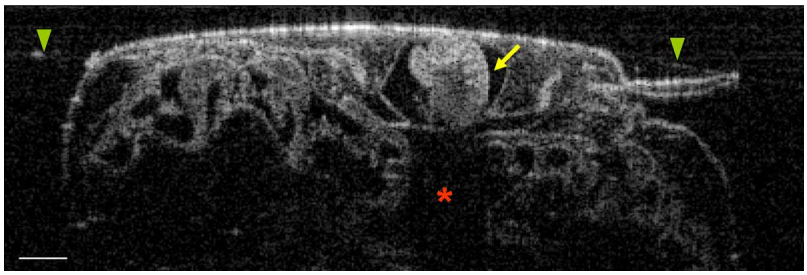

Fig. 5. (2.5 MB) A sequence of OFDI images of *Xenopus laevis* tadpole *in vivo* placed in a Petri dish filled with saline. A cross section of ventricle (yellow arrow) shows trabeculae within the chamber. Blood in the heart produces strong light scattering, resulting in a shadow region denoted by red asterisk. The saline surface produces relatively strong back reflection (green arrows), and the sample top surface is somewhat flattened due to surface tension of saline. Although the movie was acquired at 84 frames per second, it is displayed at 30 frames per second. Scale bar, 200 μm.

To demonstrate the system's capability in high-speed, high-resolution biological imaging, we obtained images of a *Xenopus laevis* tadpole *in vivo* by scanning the sample beam laterally across the sample. Immediately before imaging, an embryo (stage 48) was anesthetized using 0.02% 3-aminobenzoic acid ethyl ester (MS-222) and positioned in a Petri dish filled with saline, with its ventral surface upward. During imaging, the embryo heart was beating at a rate of approximately 2 Hz (~120 beats per minute). The sample beam has a confocal parameter of 540 μm and a FWHM beam size of 10 μm at the focus in air ($n = 1$). To maximize the resolution, we placed the focal plane in the middle of the heart. The optical power on the sample was 2.4 mW. Figure 5 shows a sequence of cross-sectional images taken as the beam was scanned laterally and repeatedly over the ventricle in the heart. The movie was acquired at a frame rate of 84.4 Hz (512 A-lines per frame) in 1.2 s, but is displayed at a reduced rate of 30 frames per second. Each frame, cropped from the original (500 x 1024 pixels), has 400 x 200 pixels and spans 3.3 mm (horizontal) by 1.1 mm (depth, $n = 1.35$). The motion of ventricle and trabeculae within are seen clearly. The ability to image a beating heart with high spatial and temporal resolution may facilitate studies of normal and abnormal cardiac development *in vivo* [27]. Combined with contrast agents, such as fluorescence dyes [28, 29] and gold nanoparticles [30] developed in the 800-nm region, the OFDI system may be useful in molecular or disease-targeted imaging with the aforementioned advantages over existing time-domain and spectral-domain systems. These studies are, however, beyond the scope of this paper.

4. Conclusion

We have developed a swept laser with a wide tuning range (55 nm) and high repetition rate (43 kHz). The tuning speed (2800 nm/ms) represents >1000-fold improvement over previously demonstrated [4] or commercially available lasers in the 800-nm region. The OFDI system we constructed using the laser source has enabled us to obtain cross-sectional

#70059 - $15.00 USD Received 18 April 2006; revised 9 June 2006; accepted 14 June 2006

images of a *Xenopus laevis* with high temporal and spatial resolutions. We expect that future engineering effort (*e.g.* reducing the 6-dB double-pass loss in the probe, enhancing the dual balancing efficiency, increasing the coherence length of the laser source) can improve the sensitivity of system. In the near future, the high-speed OFDI technology demonstrated here should prove useful in clinical ophthalmic applications and molecular contrast-based biological investigations.

Acknowledgments

This work was supported in part by the National Institute of Health through grants R33 CA110130, R01 EY14975, and R01 RR19768.

#70059 - $15.00 USD Received 18 April 2006; revised 9 June 2006; accepted 14 June 2006